

Radial Distributions of Coronal Electron Temperatures for Solar Altitudes up to Ten Solar Radii

Joseph F. Lemaire^{1,2} · Athanassios C. Katsiyannis³ 

© Springer ••••

Abstract

This paper is a follow up of the article where Lemaire and Stegen (2016) introduced a hydrodynamical (dyn) model to calculate the coronal temperature distribution ($T_e(h)$) from a given radial electron density. Several $T_e(h)$ distributions are presented here, corresponding to combinations of in-situ measurements of electron density and bulk velocity at 1 AU. The results challenge the commonly accepted view that T_e is higher close to the transition region than further away. Further more, the maximum T_e can be the double of the temperature observed at the base, making heat conductivity downwards a possibly significant phenomenon. This has serious implications to the assumption that the corona is mainly heated at its base, as it suggests that it might be happening a few solar radii higher up.

Keywords: Corona; Inner Corona, Models; Corona, Quiet; Heating; Heating, Coronal; Solar Wind; Solar Wind, Theory; Electron Density ; Electron Temperature ; Velocity Fields, Solar Wind

✉ A.C. Katsiyannis
 katsiyannis@oma.be

J.F. Lemaire
 joseph.lemaire@uclouvain.be

¹ Université Catholique de Louvain (UCL), Faculté des sciences, Place des Sciences, 2 bte L6.06.01, 1348 Louvain-la-Neuve, Belgium

² Royal Belgian Institute for Space Aeronomy, Solar-Terrestrial Centre of Excellence, Ringlaan 3, 1180, Belgium

³ Royal Observatory of Belgium, Solar-Terrestrial Centre of Excellence, Avenue Circulaire 3, 1180, Belgium

1. Introduction

Measurements of White Light (WL) brightnesses and polarisation (pB) during solar eclipses have often been used in the past to determine $n_e(h)$, the radial distribution of coronal electrons densities. Assuming approximate cylindrical symmetry of the corona around its axis of rotation, Saito *et al.* (1970, hereafter S70) constructed an two dimensional model of $n_e(h, \phi)$ as a function of the heliographic altitude, h , and latitude, ϕ . They determined this empirical model from a set of eclipse observations at epochs of minimum solar activity. S70's model has been confirmed by a few many observations since, with the most recent being figure 1b of Howard *et al.* (2019).

The density scale heights of $n_e(h)$ have generally been used to calculate coronal electron temperatures, $T_e(h)$, at given altitudes (h) and latitudes. Indeed, in the early days it was generally assumed that the coronal density decreases exponentially with h . This traditional habitual method postulates, however, that the corona is isothermal and in hydrostatic and isothermal equilibrium. The methods for calculating the coronal temperatures correspond then to the scale-height (hereafter, shm) method (van de Hulst, 1950, 1953). Nonetheless, we now know that the corona is not isothermal (Chapman and Zirin, 1957) nor in hydrostatic equilibrium, but expanding continuously outwards (Parker, 1958).

More recently, Scudder (2019) applied a verification mechanism method on four different case studies (including Alfvén (1941)'s corona temperature profile and Parker (1958)'s thermal wind model) and found serious self consistency issues. Therefore his results confirm that an alternative method has to be employed for the computation of $T_e(h)$ from $n_e(h)$ that overcomes the limitations of the previous work.

Such a method was developed by Lemaire and Stegen (2016, hereafter LS16), who called it the dyn (i.e. hydrodynamical) method. This novel approach introduced to calculate coronal temperature distributions is explained in details in section 7 of LS16 and is included below for complicity. The strength of this improved method is that it assumes a more realistic model than the hst and shm approaches, since the corona is considered in a hydrodynamical equilibrium, constantly expanding. It accepts an electron density radial distribution ($n_e(h)$) that is based on the profile first proposed by Saito *et al.* (1970) and subsequently confirmed by numerous eclipse observations. A new term was also added by LS16 to S70's $n_e(h)$ fit to account for the values measured at 1 AU:

$$n_e(h) = 10^8 [3.09 h^{-16} (1 - 0.5 \sin \phi) + 1.58 h^{-6} (1 - 0.95 \sin \phi) + 0.0251 h^{-2.5} (1 - \sqrt{\sin \phi})] + n_E (215/h)^2, \quad (1)$$

where n_E is the electron density at 1 AU, and $1 \text{ AU} \approx 215 \text{ R}_S$ (R_S is the solar radius).

The most interesting result of this new model is the coronal temperature distributions that are explained in great details in equation 16 in section 7 of LS16:

$$T(h) = -\frac{T^*}{n_e(h)} \int_h^\infty \frac{n_e(r)}{r^2} [1 + F(r)] dr, \quad (2)$$

where $F(x)$ is the ratio between the “inertial” and “gravitational” forces (equation 15 of LS16):

$$F(h) = \frac{1}{g_S R_S} h^2 u(h) \frac{d[u(h)]}{dh}. \quad (3)$$

$u(h)$ is the electron bulk velocity, g_S the gravitational acceleration on the solar surface (274 m s^{-2}) and T^* is a a normalisation temperature constant, first introduced by Alfvén (1941), set for the purposes of this paper to 17 MK.

It should be noted here that the equation 2 can produced an electron temperature profile ($T_e(h)$) for any given $n_e(h)$ distribution. This is very significant because the $T_e(h)$ can be calculated for the different $n_e(h)$ known to exist in different corona conditions (e.g. coronal holes, quiet Sun, streamers). It has already been used by Cranmer (2020) for calculating the many radial profiles of coronal temperatures and create a Monte-Carlo ensemble of several thousands of coronal electron densities. They randomly generated them for radial distances (r) ranging between 1.4 and 4 R_S (where R_S is the solar radius), with H I Ly- α measurements taken from the UVCS spectrometer on board the SOHO mission.

The aim of the present paper is to expand on the work reported by LS16 by analysing the properties of the dyn model and by applying it to different u_E and n_E observed values. The results will be compared to those of the hst and shm approaches and the physics behind those differences will be discussed. Finally, the implications of the temperature distributions produced by the dyn model to the corona heating problem will be argued.

2. Corona Electron Density Distribution in the Lower and Middle Corona

Figure 1 contains the electron density distribution introduced by different authors. It is very similar to the figure 1 of LS16 and it is included here for completion. It should be noted here that the authors do not use the radial distance, r , for the x-axis but the solar altitude, h . This choice was made to facilitate the application of a logarithmic scale, needed for the better illustration of the diverse phenomena found in the lower and middle corona ($h=r-1$). The range of h is chosen between $0.01 \leq h \leq 10 R_S$ in order to expand from the inner to the middle regions of the solar corona.

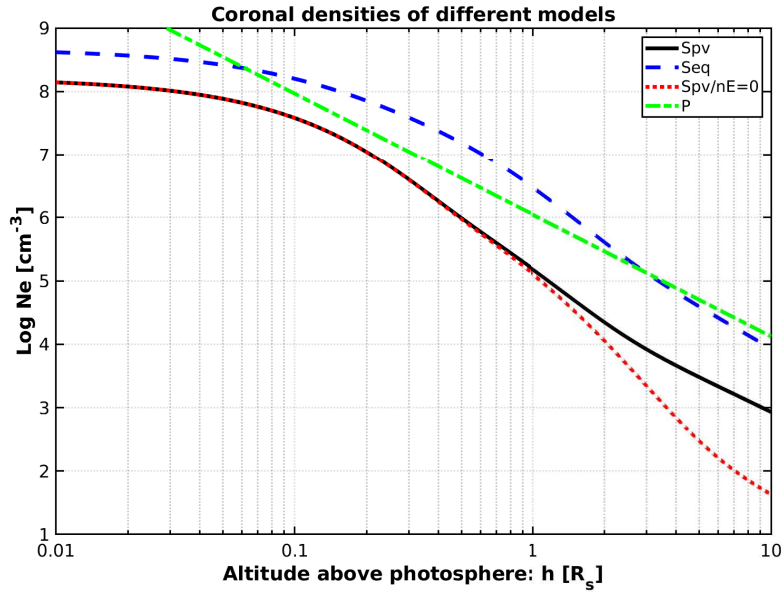


Figure 1. Expanded coronal electron density distributions for the equatorial (blue-dashed curve, Seq), and polar regions described by LS16 (black curve, Spv), taken from S70 (red dotted curve, Spv/nE=0), and from Pottasch (1960) (green-dashed-dotted curve, P). Pottasch's density distribution was also included in figure 6.5 of Parker (1963).

The black curve (Spv) corresponds to Saito's polar density distribution which has been prolonged at large distance by adding the Solar Wind density which is modelled here by :

$$n_e(h) = n_E \left(\frac{h_E}{h} \right)^2, \quad (4)$$

where n_E corresponds to the SW electron density at Earth's orbit, and h_E is 215 R_s . It is assumed that the temperature of all ions is the same as those of electrons, so no thermal energy is exchanged between barionic particles.

The difference between the red curve and the black curve in figure 1 might be regarded as the partial density of the escaping SW electrons in the exospheric models of Lemaire and Scherer (1971, 1973). Note that the population of escaping electrons compared to the populations of ballistic and trapped coronal electrons is continuously diminishing with the radial distance as expected by exospheric models. In such collisionless SW models, only the escaping supra-thermal electrons belong the class of particles which contribute to the net outward flux of electrons. Furthermore, only these supra-thermal electrons, having kinetic energies larger than the potential barrier determined by Lemaire-Scherer's polarization electric field, contribute to the net flux of energy carried out of the corona into interplanetary space. The ballistic and trapped electrons do not

contribute to these fluxes but only to the coronal and SW density and kinetic pressure.

The difference between the black and red curves in figures 1 might also be viewed as the escaping electrons contributing to the evaporation flux in other collisional kinetic models of the SW. The review paper by Echim, Lemaire, and Lie-Svendsen (2011) contains a summary of those models in Section 4.6, that are based on the Fokker-Planck equation (see also Lie-Svendsen, Hansteen, and Leer (1997); Pierrard, Maksimovic, and Lemaire (1999, 2001)). They are currently the most advanced kinetic-based paradigm for the SW. In contrast, the MHD models of the SW do not make any distinction between the sub-thermal and the supra-thermal electrons and hence no estimation is made on their contribution (or lack of) to these net fluxes. This is clearly an important difference in approach between all hydrodynamic/fluid and kinetic/exospheric models of the SW.

The red-dotted curve ($Spv/nE=0$) might be regarded as corresponding to the sum of densities of the ballistic and trapped electrons. Those particles do not have a high enough kinetic energy to escape out the Lemaire-Scherer coronal electrostatic potential determined in the early kinetic SW models (Lemaire and Scherer, 1971, 1973). The blue-dashed curve (Seq) in figure 1 corresponds to S70's expanded equatorial density model (i.e. $\phi = 0$).

The green curve (P) in figure 1 corresponds to a best fit of the equatorial electron density distribution during solar minimum by Pottasch (1960). It was produced by WL brightness and polarization measurements during a solar eclipse of 1952 and the assumption of a hydrostatic model. It can be clearly seen that all the S70 and Pottasch (1960) fits of observational data differ very significantly from the usual critical solutions of the SW hydrodynamic transport equations. This is for instance well illustrated in figure 1 of Scarf and Noble (1965) and in later models. To our best knowledge this important difference has been consistently overlooked for many decades.

3. The Dyn Electron Temperature Profile Properties

S70's equatorial and polar density distributions shown in figure 1 have been employed to calculate the electron temperatures by using all three different methods (hst, shm, and dyn) described by LS16. These temperatures profiles are shown in figure 2 for the polar regions. Similar temperature profiles were displayed in figure 3 of LS16, but for the equatorial regions of the Corona. The hst curve shown here is more similar to the fit carefully derived by Alfvén (1941) than those by later authors. The comparison of these two figures shows that in both regions the maximum of the shm temperature is always located at higher altitudes than the maximum of the hst temperature. Interestingly enough, these two peak temperatures have almost the same values (circa 1 MK) whatever the method of calculation (shm or hst) is used to determine the $T_{e,\max}$. This agreement between all the pre-LS16 models created an impression of certainty for the value of $T_{e,\max}$ in the middle corona, yet, this is now challenged by LS16 and this work.

In both figures (i.e. 2 and LS16's figure 3) the dyn and hst methods give almost identical temperatures distributions at the base of the corona, as in such

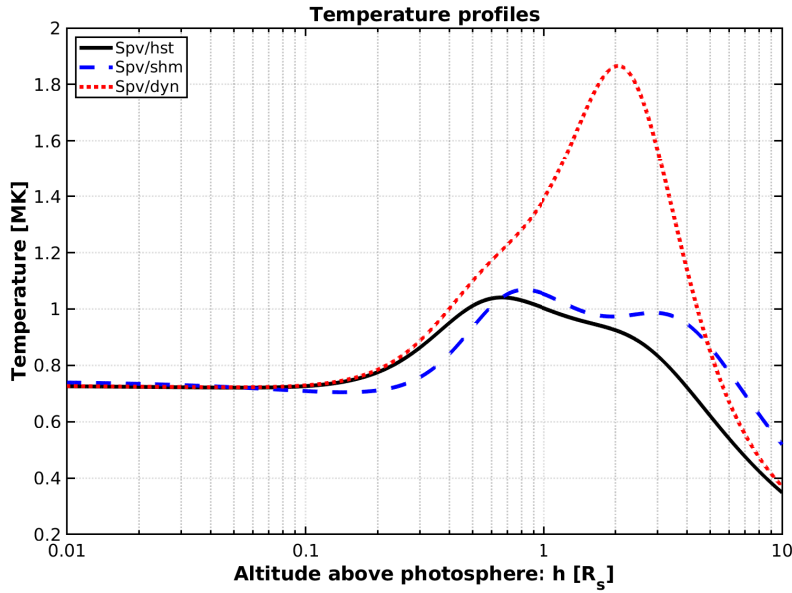


Figure 2. The electron temperature profiles over the polar regions (Spv) calculated by the three different methods: The scale height (shm), the hydrostatic (hst), and the hydrodynamical (dyn, introduced by LS16). All three curves are calculated with the same polar electron density profile (Spv; the black curve in figure 1) for which $n_E = 2.2 \text{ cm}^{-3}$ at 1 AU. The red-dotted curve (Spv/dyn) is obtained by assuming that the SW velocity at 1 AU is equal to $u_E = 329 \text{ km/s}$ (which is the most typical value), while the solid black curve (Spv/hst) is obtained for $u_E = 0$ (as the hydrodynamical model then becomes hydrostatic).

low altitudes $u(h) \approx 0$. Significant differences only appear gradually and in the middle corona the two profiles differ drastically. It should also be noted that $u(h)$ plays such a significant role in the temperature distribution because it remains subsonic up until $\approx 10 R_S$. This explains why $T_e(h)$ becomes again almost identical for the two models for large solar altitudes.

However, it is important to emphasise on the difference between the equatorial and polar profiles calculated from the dyn model. For low latitudes the hst and dyn temperature estimations depart from each-other at higher altitudes than in the poles or CHs ($h \gtrsim 1 R_S$ and $h \gtrsim 0.5 R_S$ respectively) and never produce the drastic differences in T_e . As such in the future it will easier to confirm the validity of the dyn model from observations of the poles and CHs than of the equatorial region.

Above the transition region (i.e. for $h \in [0.003 R_S, 0.1 R_S]$), all calculated temperatures tend to almost constant values. This means that at the base of the solar Corona the plasma tends always to become almost isothermal. But these near isothermal values of $T_e(h)$ are clearly much larger over the equatorial regions (1.03 MK) than over the poles (0.72 MK). This prediction of the dyn model is also fully consistent with the well known observations reported in <https://solarscience.msfc.nasa.gov/Skylab.shtml>.

All gases in isothermal equilibrium must have the polytropic index, γ , equal to unity (i.e. $p \propto \rho$). Thus, for the polar region (or CHs) and altitudes below 0.1 R_S , we have:

$$\gamma = 1 + \frac{\frac{\partial}{\partial r} \log(n_e)}{\frac{\partial}{\partial r} \log(T_e)} \cong 1.1. \quad (5)$$

Another very important difference between the hst and dyn methods is altitude of the maximum T_e , h_{\max} . As it can be seen from figure 2, the former produces a lower h_{\max} ($\approx 0.65 R_S$) than the latter ($\approx 2.09 R_S$). The consequences of this is that the fast SW flows (lets say $u_E = 500$ km/s) require a high T_e (reaching a maximum of 1.89 MK in this example) in the region of $1.0 \leq h \leq 10 R_S$, but it will not have a significant effect in the temperature distribution for $h \leq 10 R_S$ (which remains at ≈ 0.72 MK in this model). Hence, there is no inconsistency between the dyn model and the plethora of existing low corona observations that measure electron temperatures unaffected by variations of the SW velocity.

It is also worth mentioning that the dyn model produces different profiles for the equatorial and polar/CHs regions, since it allows for different input u_e ab ovo. This is in contrast to the hst and shm methods that do not incorporate in-situ measurements at 1 AU. As can be seen from the comparison between the figure 3 of LS16 and figure 2, $T_{e,\max}$ is much larger over the poles (or CHs), with $T_e(2 R_S) \approx 1.9$ MK than in the equatorial plane where it peaks at $T_e(0.27 R_S) \approx 1.4$ MK.

4. The Correlation Between Higher Coronal Electron Temperatures, n_E , and u_E

Figure 3 displays the dyn temperature profiles based on the equatorial electron density, $n_e(r)$, of figure 1 which in turn is obtained from Saito's extended density model for $\phi = 90^\circ$. They are calculated by integrating numerically equations 2 and 3, where $u(h)$ is determined by:

$$u(h) = u_E \frac{A_E}{A(h)} \frac{n_E}{n_e(h)}. \quad (6)$$

Equation 6 is derived from the equation of conservation of particle flux, where $A(h)$, is the cross-section of flow tubes, first introduced by Kopp and Holzer (1976) (also see equation (12) in LS16). For the purposes of this paper, it is assumed that $A_E/A(h) = 1$, i.e. there is no radial expansion of the corona flow tubes. Although this is clearly not the case, it is considered that for altitudes below $10 R_S$ this ratio is close to 1, hence it has been omitted for simplicity.

The solid-black curve figure 3 has been obtained $u_E = 329$ km/s and $n_E = 5.75 e^-/\text{cm}^3$. These input parameters are respectively the SW bulk velocity and number density at 1 AU of the average slow SW flow, as reported by Ebert *et al.* (2009). The other three profiles refer to temperatures for increasing values of

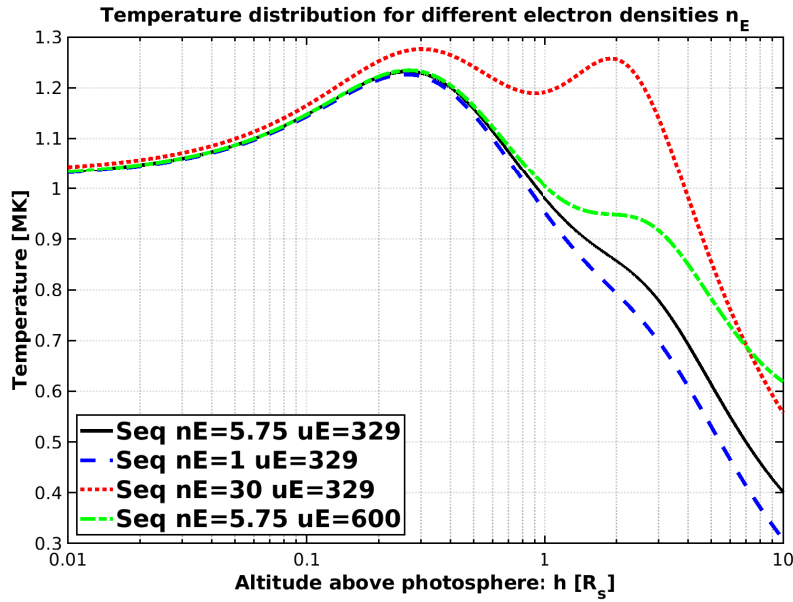


Figure 3. Equatorial distributions of the dyn temperature obtained with the following combinations of SW bulk velocity and electron density at 1 AU: $n_E = 1 \text{ e}^-/\text{cm}^3$, $u_E = 329 \text{ km/s}$ (blue dashed line); $n_E = 5.75 \text{ e}^-/\text{cm}^3$, $u_E = 329 \text{ km/s}$ (black solid line); $n_E = 30 \text{ e}^-/\text{cm}^3$, $u_E = 329 \text{ km/s}$ (red dotted line); and $n_E = 5.75 \text{ e}^-/\text{cm}^3$, $u_E = 600 \text{ km/s}$ (dashed-green line).

n_E and u_E that remain, however, within the observed range. According to these results, larger electron temperatures are needed in the middle corona in order to accelerate the SW flows whose density (n_E) or velocity (u_E) is larger than the typical values. More importantly, large variation in n_E produce less significant differences in $T_e(h)$ than more moderate variations in u_E . As a consequence, the dyn model favours an enhanced heating rate over a less dense plasma as the evidence point toward a more close connection between heating and bulk velocity in the SW rather than heating and electron density.

5. Discussion

The temperature distribution described here and in LS16 is determined as a solution of the momentum density transport equation, resulting in a $T_e(r)$ with a totally different distribution to that of the critical solutions of the one-fluid or two-fluids hydrodynamical transport equations adopted by other authors. Those singular solutions predict that $\partial[\log T_e(r)]/\partial r$ tends to a negative value when $r \rightarrow 1 R_s$. Although never pointed out before, the very existence of a negative temperature gradient at the top of the chromospheric region is difficult to justify from the physical point of view. On the contrary, all temperature profiles of the dyn model predict a very slow temperature increase for the altitudes just above the transition region.

Albeit in the present paper we do not discuss possible coronal heating mechanisms that should be able to account for the temperature profiles shown in figures 2 and 3, it is worth pointing out that these profiles have their maximum in the mid corona, well above the transition region ($h_{tr} \approx 0.003 R_S$). This implies that the altitude of the maximum of coronal heating rate is expected well above the transition region, unlike what is predicted by traditional hydrodynamical SW models proposed in the past.

Furthermore, the electron density scale height at the base of the corona predicted by the above mentioned critical hydrodynamical solutions of SW models, is always larger than the actual scale heights determined from WL eclipse observations. This is illustrated in figure 1 of Scarf and Noble (1965) where the theoretical electron density distributions of $n_e(h)$ determined by the critical solution of the Navier-Stokes transport equations were compared to those derived experimentally from several eclipse measurements. This uncomfortable disagreement was pointed out by the authors of this early study of one-fluid SW hydrodynamical models (Scarf and Noble, 1965). Surprisingly this grievous discrepancy between the theoretical density gradient derived from the critical solutions of hydrodynamical SW models and the actual electron density gradients (or scale heights) has never again been pointed out in later discussions of the limitations of hydrodynamical SW models (Parker, 1958, 1963).

6. Conclusions

Having recalled LS16's dyn model that was used to calculate the radial distributions of coronal electron temperatures ($T_e(r)$) for a given electron density distribution ($n_e(r)$), we have employed the same method to calculate the electron temperatures as a function of altitude in the equatorial and polar regions for different given input parameters: the solar wind density (n_E) and the expansion velocity (u_E) at 1 AU. The calculated temperature distributions have been compared with those determined by using other methods of calculation, namely, the scale-height (shm) and the hydrostatic (hst) methods which are commonly used and assume a corona in isothermal and in hydrostatic equilibrium respectively.

It is found that, in all cases the calculated temperature has a maximum value at an altitude, h_{max} , which is much higher than the altitude of the transition region. This is a very important result of the dyn model since it implies that the corona heating does not happen just above the transition region, as it has always been assumed, but much higher (of the order of a few solar radii).

Even more, this work and LS16 has calculated that the maximum electron temperature ($T_{e,max}$) is not of the order of 1 MK as computed by the hst and shm models, but much higher (for example 1.8 MK for typical polar conditions). This has very serious implications since it has always been assumed that all models converge to a temperature of 1 MK, hence creating a false sense of certainty about this value almost universally in literature. Additionally, it has been shown that this maximum value is positively correlated to the measurements of SW electron density, n_E , and bulk velocity, u_E , at 1AU. If true, this may play a very significant role in the attempts to connect the SW condition observed at lower corona with

the in-situ measurements at 1 AU. It is now clear that the dyn model predicts significantly higher temperatures in the $1.0 \leq h \leq 10 R_S$ region when either n_E or u_E is higher. As such, larger heating rates are required in the middle corona to boost the plasma to larger supersonic velocities and higher density observed at 1AU.

For the altitude range of (i.e. $h < 0.1 R_S$) the calculated dyn temperatures approach almost constant values which are larger over the equatorial regions (circa 1-1.2 MK) than over the poles (circa 0.7 MK).

Nevertheless, LS16 have also shown that the radial distribution of the electron temperature depends critically on the ratio of the concentrations of heavier coronal ions (He^{++} , etc) and on the ion temperature distributions under certain conditions. In this work, the authors have assumed the ion temperature to be equal to that of the electrons and no contribution from heavier ions. These assumptions are probably satisfactory at low altitudes where Coulomb collisions play a much stronger role than at higher altitudes. Even more, the recent eclipse observations of Koutchmy *et al.* (2019) seem to support for $h < 5 R_S$ the proton and electron temperatures might be equal, but this remains a hypothesis that needs to be more thoroughly verified (possibly with data collected during the PSP and Solar Orbiter missions). Higher up such simplifying assumptions are becoming lapsed, as shown in the ion-exospheric models of Lemaire and Scherer (1971, 1973). Future work will study the effect of the heavier coronal ions and of the potential differences of the temperature distributions of electrons and protons.

Acknowledgments We acknowledge the logistic support of BELSPO the Belgian Space Research Office, as well as the help of the IT teams of BIRA and ROB. JFL wishes also to thanks Viviane Pierrard (BIRA-IASB), Marius Echim (BIRA-IASB), and Koen Stegen (ROB). We acknowledge Serge Koutchmy for his interest in our work, and for pointing out in page 3664 of Lemaire and Stegen (2016) an unfortunate but non consequential mistake in the given numerical value of H (the density scale height at the base of the Corona when the temperature is assumed to be equal to 1 MK). ACK acknowledges funding from the Solar-Terrestrial Centre of Excellence (STCE), a collaborative framework funded by the Belgian Science Policy Office (BELSPO). Some work for this paper was also done in the framework of the SOL3CAM project (Contract: BR/154/PI/SOL3CAM), funded by BELSPO.

The authors are not aware of any conflicts of interest. The authors have no relevant financial or non-financial interests to disclose. All work done for this article was funded by the Royal Belgian Institute for Space Aeronomy (BIRA-IASB), the Université Catholique de Louvain (UCL), Belgium, and the Royal Observatory of Belgium (ROB). Both royal institutes are funded by the BELgian Science Policy Office (BELSPO). J. F. Lemaire is an emeritus professor of UCL and a retired researcher of BIRA-IASB. All work for this article was done after his retirement. A. C. Katsiyannis is an employee of ROB and also a member of the STCE. All his work for this articles was done while an ROB/STCE employee.

References

Alfvén, H.: 1941, On the solar corona. *Ark. Mat. Astron. Fys.* **27**, 1.
 Chapman, S., Zirin, H.: 1957, Notes on the Solar Corona and the Terrestrial Ionosphere. *Smithsonian Contributions to Astrophysics* **2**, 1. ADS.
 Cranmer, S.R.: 2020, Heating Rates for Protons and Electrons in Polar Coronal Holes: Empirical Constraints from the Ultraviolet Coronagraph Spectrometer. *ApJ* **in press**.

Ebert, R.W., McComas, D.J., Elliott, H.A., Forsyth, R.J., Gosling, J.T.: 2009, Bulk properties of the slow and fast solar wind and interplanetary coronal mass ejections measured by Ulysses: Three polar orbits of observations. *Journal of Geophysical Research (Space Physics)* **114**(A1), A01109. DOI. ADS.

Echim, M.M., Lemaire, J., Lie-Svendsen, Ø.: 2011, A Review on Solar Wind Modeling: Kinetic and Fluid Aspects. *Surveys in Geophysics* **32**(1), 1. DOI. ADS.

Howard, R.A., Vourlidas, A., Bothmer, V., Colaninno, R.C., DeForest, C.E., Gallagher, B., Hall, J.R., Hess, P., Higginson, A.K., Korendyke, C.M., Kouloumvakos, A., Lamy, P.L., Liewer, P.C., Linker, J., Linton, M., Penteado, P., Plunkett, S.P., Poirier, N., Raouafi, N.E., Rich, N., Rochus, P., Rouillard, A.P., Socker, D.G., Stenborg, G., Thernisien, A.F., Viall, N.M.: 2019, Near-Sun observations of an F-corona decrease and K-corona fine structure. *Nature* **576**, 232. DOI. ADS.

Kopp, R.A., Holzer, T.E.: 1976, Dynamics of coronal hole regions. I. Steady polytropic flows with multiple critical points. *Solar Phys.* **49**(1), 43. DOI. ADS.

Koutchmy, S., Baudin, F., Abdi, S., Golub, L., Sèvre, F.: 2019, New deep coronal spectra from the 2017 total solar eclipse. *Astron. Astrophys.* **632**, A86. DOI. ADS.

Lemaire, J., Scherer, M.: 1971, Kinetic models of the solar wind. *J. Geophys. Res.* **76**(31), 7479. DOI. ADS.

Lemaire, J., Scherer, M.: 1973, Kinetic models of the solar and polar winds. *Reviews of Geophysics and Space Physics* **11**, 427. DOI. ADS.

Lemaire, J.F., Stegen, K.: 2016, Improved Determination of the Location of the Temperature Maximum in the Corona. *Solar Phys.* **291**(12), 3659. DOI. ADS.

Lie-Svendsen, Ø., Hansteen, V.H., Leer, E.: 1997, Kinetic electrons in high-speed solar wind streams: Formation of high-energy tails. *J. Geophys. Res.* **102**(A3), 4701. DOI. ADS.

Parker, E.N.: 1958, Suprathermal Particles. III. Electrons. *Physical Review* **112**(5), 1429. DOI. ADS.

Parker, E.N.: 1963, *Interplanetary dynamical processes*. ADS.

Pierrard, V., Maksimovic, M., Lemaire, J.: 1999, Electron velocity distribution functions from the solar wind to the corona. *J. Geophys. Res.* **104**(A8), 17021. DOI. ADS.

Pierrard, V., Maksimovic, M., Lemaire, J.: 2001, Self-consistent model of solar wind electrons. *J. Geophys. Res.* **106**(A12), 29305. DOI. ADS.

Pottasch, S.R.: 1960, Use of the Equation Hydrostatic Equilibrium in Determining the Temperature Distribution in the Outer Solar Atmosphere. *Astrophys. J.* **131**, 68. DOI. ADS.

Saito, K., Makita, M., Nishi, K., Hata, S.: 1970, A non-spherical axisymmetric model of the solar K corona of the minimum type. *Annals of the Tokyo Astronomical Observatory* **12**(2), 51. ADS.

Scarf, F.L., Noble, L.M.: 1965, Conductive Heating of the Solar Wind. II. The Inner Corona. *Astrophys. J.* **141**, 1479. DOI. ADS.

Scudder, J.D.: 2019, The Long-standing Closure Crisis in Coronal Plasmas. *Astrophys. J.* **885**(2), 148. DOI. ADS.

van de Hulst, H.C.: 1950, The electron density of the solar corona. *bain* **11**, 135. ADS.

van de Hulst, H.C.: 1953, In: Kuiper, G.P. (ed.) *The Chromosphere and the Corona*, 207. ADS.